Enhanced thermal conductivity and isotope effect in single-layer hexagonal boron nitride

L. Lindsay[1] and D. A. Broido[2,*]

[1]*Naval Research Laboratory, Washington, D.C. 20735, USA*

[2]*Department of Physics, Boston College, Chestnut Hill, Massachusetts 02467, USA*

(Received 25 August 2011; revised manuscript received 23 September 2011; published 13 October 2011)

The thermal conductivity, κ, of single layers of hexagonal boron nitride (h-BN), as well as that of bulk h-BN have been calculated utilizing an exact numerical solution of the phonon Boltzmann transport equation. The stronger phonon-phonon scattering in h-BN is revealed as the cause for its lower κ compared with graphite. A reduction in such scattering in the single layer arising mainly from a symmetry-based selection rule leads to a substantial increase in κ, with calculated room temperature values of more than 600 $\mathrm{Wm^{-1}K^{-1}}$. Isotopic enrichment further increases κ, with the calculated enhancement exhibiting a peak with temperature, whose magnitude shows a dramatic sensitivity to crystallite size.

DOI: 10.1103/PhysRevB.84.155421 PACS number(s): 63.20.kg, 63.22.Rc, 66.70.−f, 65.80.Ck

I. INTRODUCTION

Single-layer hexagonal boron nitride (SLBN) is structurally analogous to graphene, but with carbon atoms replaced by alternating boron and nitrogen atoms. In the shadow of graphene, SLBN and multilayer hexagonal boron nitride (MLBN) are now receiving increased attention because of their promise for a number of applications, such as substrates for graphene electronics.[1,2]

Understanding the lattice thermal conductivities, κ_L, of these materials will be important when coupling them to nanoscale electronics and will provide additional insight into the novel behavior of phonon transport in 2D layered structures.[3–9] The highest recorded room temperature thermal conductivity of bulk hexagonal boron nitride (h-BN) is around 400 $\mathrm{Wm^{-1}K^{-1}}$[10] which is five times lower than that of pyrolytic graphite.[11] This is surprising given the similar crystal structures, lattice constants, unit cell masses, and phonon dispersions shared by these materials. One notable difference between the two is that h-BN has a significantly larger isotope mixture (19.9% ^{10}B, 80.1% ^{11}B) than graphite (98.9% ^{12}C, 1.1% ^{13}C), causing stronger phonon-isotope scattering, as indicated by the large isotope effect recently observed in boron nitride nanotubes (BNNTs).[12] At the same time, the observed decrease of κ_{hBN} with increasing temperature around 300 K[10] is a signature that intrinsic phonon-phonon scattering due to lattice anharmonicity is the dominant scattering mechanism limiting κ_L, as is the case in most semiconductors and insulators.

These observations suggest that to understand the κ_L in SLBN as well as h-BN, a rigorous microscopic thermal transport theory is needed that simultaneously incorporates both phonon-phonon scattering and that by isotopes. In this paper, we present such a theory based on an exact numerical solution of the Boltzmann transport equation (BTE) for phonons,[5,7,13] which is necessary to treat the inelastic nature of the phonon-phonon scattering accurately. Our approach reveals that SLBN possesses unusual transport properties similar to those recently identified in graphene.[5,7] In particular, the majority of heat is carried by acoustic phonons vibrating perpendicular to the layer plane (the so-called ZA phonons), a finding that contradicts early predictions[14,15] but is consistent with recent thermal transport measurements on graphene structures.[5,6,16] We find that around room temperature, phonon-phonon scattering is stronger in SLBN (h-BN) than in graphene (graphite), explaining the observed difference in κ_L for these systems. However, the κ_L of SLBN is found to be considerably larger than κ_{hBN} (bulk value), with room temperature values of more than 600 $\mathrm{Wm^{-1}K^{-1}}$, one of the highest among non-carbon-based materials. This enhancement is connected to a symmetry-based selection rule that strongly suppresses phonon-phonon scattering in 2D crystals.[5,7] Finally, we show that the interplay between phonon-phonon scattering and that by isotopes leads to a strongly temperature dependent isotope effect, with peak enhancements in κ_L depending sensitively on crystallite sizes.

In Sec. II, the lattice thermal conductivity and its constituents to be calculated are introduced. Sec. III describes the empirical interatomic potential developed for h-BN systems, from which the harmonic and anharmonic interatomic force constants are obtained, and it demonstrates the accuracy of this potential in describing the acoustic phonon frequencies and velocities. The scattering rates for phonon-phonon, isotope impurity, and boundary scattering are presented in Sec. IV, along with a summary of the approach to solve the phonon BTE. Section V presents our results and an accompanying discussion, and Sec. VI provides a summary and our conclusions.

II. THERMAL CONDUCTIVITY

While significant progress has been made in the fabrication of SLBN and MLBN,[17–19] there is currently no measured κ_L data for these systems. To connect our theory to experiment, we have calculated κ_L not only for SLBN but also for MLBN. As was found previously for multilayer graphene,[13] with increasing layer number, N, the calculated κ_L of MLBN saturates to an N-independent value after only five layers. Thus, the κ_L for $N = 5$ is taken as the calculated κ_{hBN}, which is compared directly to that determined experimentally.[10]

We consider the h-BN layers to be parallel to the x-y plane with thermal reservoirs at slightly different temperature taken to be separated along the x-direction, chosen to be along $\Gamma \rightarrow M$ of the 2D hexagonal Brillouin zone. The κ_L for SLBN and

MLBN is given by:

$$\kappa_L = \frac{1}{(2\pi)^2(N\delta)} \sum_j \int \left(\partial n^0_\lambda / \partial T\right) \hbar \omega_\lambda v^2_{\lambda x} \tau_\lambda d\mathbf{q} \qquad (1)$$

In Eq. (1), δ is the interlayer spacing and ω_λ is the frequency of a phonon in mode $\lambda = (\mathbf{q}, j)$ with wavevector $\mathbf{q} = (q_x, q_y)$ and with branch index j, n^0_λ is the Bose distribution function, $v_{\lambda x} = d\omega_\lambda / dq_x$ is the component of the phonon velocity along the direction of thermal transport, and τ_λ is the phonon lifetime in this mode.

Note that we have taken the thermal conductivity to be a scalar, reflecting that the in-plane transport is isotropic. This is indeed the case for an infinite 2D hexagonal lattice. For finite systems, in principle, the thermal conductivity would exhibit a directional ansiotropy. However, for the relatively large size systems here, this anisotropy is small (<5%), and we ignore it in the present work.

III. INTERATOMIC FORCE CONSTANTS

To calculate the phonon frequencies, velocities, and lifetimes in (1), a description of the harmonic and anharmonic interatomic forces is required. Here we use a Tersoff empirical interatomic potential[20] to describe the in-plane bonding between atoms. A new set of Tersoff potential parameters for h-BN was determined using a least squares fitting procedure so as to best fit the measured in-plane acoustic phonon dispersion data of bulk h-BN,[21] as well as the in-plane bond length[22] and cohesive energy.[23] The approach is identical to that used previously for graphene.[24] Unlike graphene, which has purely covalent bonding between carbon atoms, the h-BN bonding is also partly ionic. However, the resulting interatomic Coulomb interaction affects primarily the optic phonon frequencies near the zone center.[25] Because our interest is in the acoustic phonon branches, which are most important for thermal transport, we ignore this Coulomb term. For the weak interlayer bonding, a Lennard–Jones (L-J) potential is used: $V_{LJ}(r_{ij}) = 4\varepsilon[(\sigma/r_{ij})^{12} - (\sigma/r_{ij})^6]$, where r_{ij} is the distance between atoms i and j in adjacent layers, and ε and σ were adjusted to match the measured interplanar distance of $\delta = 0.333$ nm[22] and to best fit the z-axis phonon dispersion. We have used an AA′ stacking of h-BN layers, which is consistent with that found in recent ab initio calculations.[26] The optimized Tersoff and L-J potential parameters are listed in Table I.

The phonon frequencies and velocities for MLBN with N layers are calculated by diagonalizing $6N \times 6N$ dynamical matrices using harmonic interatomic force constants obtained from the Tersoff and L-J potentials. The Tersoff potential includes up to second nearest neighbor interactions, whereas we include up to third nearest neighbor interactions between atoms in adjacent planes. The calculated phonon dispersion for bulk h-BN is shown in Fig. 1 (black curves) compared with the measured values from Ref. 21. A very good fit is obtained for the low-frequency portion of the phonon spectrum. In particular, the quadratic ZA phonon branch and the transverse acoustic (TA) and longitudinal acoustic (LA) branches are accurately represented. Table II shows that the lattice constants, cohesive energy, and acoustic velocities are in close agreement with measured values. In particular, the TA and LA velocities are within 5% of those obtained from the measured dispersions.[21]

TABLE I. Optimized Tersoff and Lennard-Jones parameters for h-BN systems.

$A = 1433.0$ eV	$B = 417.30$ eV
$\lambda_1 = 3.4661$ Å^{-1}	$\lambda_2 = 2.2288$ Å^{-1}
$\lambda_3 = 0.0000$ Å^{-1}	$n = 0.72674$
$c = 30692.4$	$\beta = 1.0239 \times 10^{-7}$
$d = 4.7295$	$h = -0.98578$
$R = 1.95$ Å	$D = 0.15$ Å
$\varepsilon = 0.004$ eV	$\sigma = 0.3212$ nm

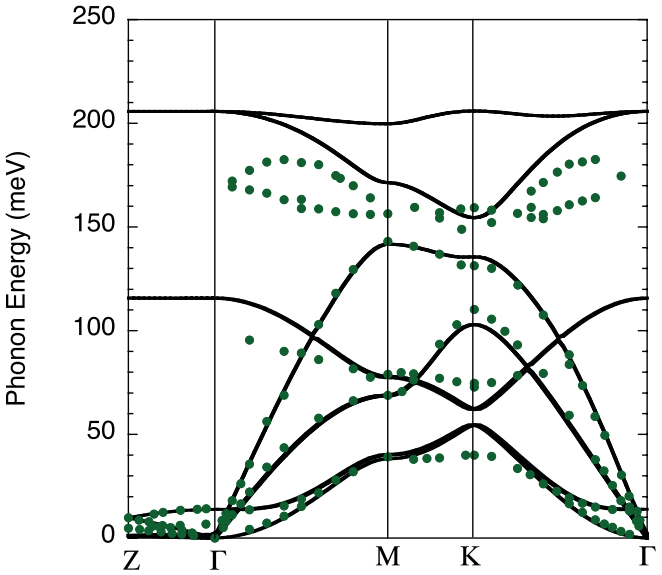

FIG. 1. (Color online) Phonon dispersion given by the optimized Tersoff potential for bulk h-BN (black curves) compared with measured data (green circles) [Ref. 21].

IV. THERMAL TRANSPORT THEORY

The phonon lifetimes, τ_λ, are calculated from an exact numerical solution to the phonon BTE.[5,7,13] They are limited by phonon-phonon, isotopic impurity, and boundary scattering. The dominant phonon-phonon scattering processes are those between three phonons. Higher order processes have been estimated to be much weaker, even up to much higher

TABLE II. Lattice constants, cohesive energy, and acoustic phonon velocities for in-plane bulk h-BN as given by the Tersoff potential compared with experiment.

	Experiment	Tersoff/L-J Model
a_{lat} (Å)	2.50[a]	2.50
c_{lat} (Å)	6.66[a]	6.65
E_{coh} (eV)	−8.09[b]	−8.04
v_{TA} (m/s)	11496[c]	10890
v_{LA} (m/s)	19145[c]	19157

[a]Reference 22.
[b]From ab initio calculation, Ref. 23.
[c]From dispersion, Ref. 21.

temperatures than considered here.[27] Therefore, in this work, we consider the lowest order three-phonon scattering only. The three-phonon scattering rates can be expressed as

$$1/\tau_\lambda^{\rm anh} \equiv \sum\nolimits_{(+)} \Gamma^{(+)}_{\lambda\lambda'\lambda''} + 1/2 \sum\nolimits_{(-)} \Gamma^{(-)}_{\lambda\lambda'\lambda''}, \qquad (2)$$

where the sums are over the phase space of all three-phonon processes satisfying the conservation of energy and momentum—$\omega_j(\mathbf{q}) \pm \omega_{j'}(\mathbf{q}') = \omega_{j''}(\mathbf{q}'')$ and $\mathbf{q} \pm \mathbf{q}' = \mathbf{q}'' + \mathbf{K}$—where $\mathbf{K}$ is a reciprocal lattice vector of the 2D hexagonal lattice. This phase space is calculated on a fine grid in $\mathbf{q}$ space, including both Normal ($\mathbf{K} = 0$) and Umklapp ($\mathbf{K} \neq 0$) processes. In (2),

$$\Gamma^{(\pm)}_{\lambda\lambda'\lambda''} = \frac{\hbar\pi}{4N_0\omega_\lambda\omega_{\lambda'}\omega_{\lambda''}} \left\{ \begin{matrix} n^0_{\lambda'} - n^0_{\lambda''} \\ n^0_{\lambda'} + n^0_{\lambda''} + 1 \end{matrix} \right\} \times \left|\Phi^{(\pm)}_{\lambda,\pm\lambda',-\lambda''}\right|^2 \delta(\omega_\lambda \pm \omega_{\lambda'} - \omega_{\lambda''}), \qquad (3)$$

where N_0 is the number of unit cells in the crystal, and the three-phonon scattering matrix elements are[5,7,13]

$$\Phi_{\lambda\lambda'\lambda''} = \sum_\kappa \sum_{l'\kappa'} \sum_{l''\kappa''} \sum_{\alpha\beta\gamma} \Phi_{\alpha\beta\gamma}(0\kappa, l'\kappa', l''\kappa'') \times \frac{e^\lambda_{\alpha\kappa} e^{\lambda'}_{\beta\kappa'} e^{\lambda''}_{\gamma\kappa''}}{\sqrt{M_\kappa M_{\kappa'} M_{\kappa''}}} e^{i\mathbf{q}'\cdot\mathbf{R}_{l'}} e^{i\mathbf{q}''\cdot\mathbf{R}_{l''}}. \qquad (4)$$

Here, $l\kappa$ designates the κth atom (with mass M_κ) in the lth unit cell, $\Phi_{\alpha\beta\gamma}(0\kappa, l'\kappa', l''\kappa'')$ are third-order anharmonic interatomic force constants obtained from the Tersoff and L-J potentials, $\mathbf{R}_l$ are lattice vectors, and $e^\lambda_{\alpha\kappa}$ are phonon eigenvectors.

Because of the large concentration of ^{10}B atoms (19.9%) in the more abundant ^{11}B atoms (80.1%) in naturally occurring boron, isotopic impurity scattering is crucially important to understanding the lattice thermal transport in BN systems. We treat the isotope impurity scattering using perturbation theory.[28] The scattering rate is

$$1/\tau^{\rm iso}_\lambda = \frac{\pi}{2N_0}\omega^2_\lambda \sum_{\lambda'} \left(\sum_\kappa g_\kappa \left|\hat{e}^\lambda_\kappa \cdot \hat{e}^{\lambda'*}_\kappa\right|^2 \right) \delta(\omega_\lambda - \omega_{\lambda'}), \qquad (5)$$

where $g_\kappa = \sum_i f_{i\kappa}(\Delta M_{i\kappa}/\bar{M}_\kappa)^2$ is the mass variance parameter,[28] with i representing the two different isotope types; $f_{i\kappa}$ is the fraction of such isotopes; and $\Delta M_{i\kappa}$ is the mass difference of the isotopes from the average, $\bar{M}_\kappa$. The nitrogen in h-BN is almost pure ^{14}N, so we take $g_N = 0$, with the natural B isotope concentrations, $g_B = 0.001366$.

The high impurity concentration in naturally occurring h-BN systems raises the question of the importance of coherent scattering. For boron nitride nanotubes,[29] it has been shown that multiple scattering effects lead to only modestly higher thermal conductivity than predicted by the independent scatterer model used here. Furthermore, recent calculations of thermal transport in carbon nanotubes[30] with isotopic disorder show good agreement between results obtained using BTE and Greens function approaches, demonstrating the accuracy of the former approach even for high isotope concentrations.

In h-BN and graphite, phonons scatter from crystallite boundaries,[10] so crystallite size is an important factor in determining κ_L. The scattering rate due to crystallite boundaries is taken to be, $1/\tau^{bs}_\lambda = 2|v_{\lambda x}|/L$, where L is a measure of the length between boundaries in the transport direction. This form gives the correct limits of κ_L for nanotubes[31] and nanoribbons[32] in the ballistic ($L \to 0$) and diffusive ($L \to \infty$) limits. For the crystallite sizes considered here ($L \sim$ 1–10 μm), almost the same results are obtained using the more conventional relation $1/\tau^{bs}_\lambda = |v_\lambda|/L_{\rm eff}$ ($|v_\lambda| = \sqrt{v^2_{\lambda x} + v^2_{\lambda y}}$), with the choice $L_{\rm eff} = L/\sqrt{2}$. This follows from the isotropy of transport in an infinite 2D hexagonal lattice, so that $\langle v^2_\lambda \rangle = 2\langle v^2_{\lambda x} \rangle$.

Millions of Normal and Umklapp processes are calculated to represent the three-phonon scattering rates accurately (Eqs. (2) and (3)). Using these scattering rates, the phonon BTE is solved with an iterative approach identical to that presented previously for graphene systems.[5,7,13] The standard relaxation time approximation (RTA): $\tau^0_\lambda = (1/\tau^{\rm anh}_\lambda + 1/\tau^{\rm iso}_\lambda + 1/\tau^{bs}_\lambda)^{-1}$ gives much lower κ_L than the exact solution of the phonon BTE in 2D-layered systems because of the unusually strong Normal scattering processes involving ZA phonons, which are incorrectly treated as resistive in the RTA.[7,13]

V. RESULTS AND DISCUSSION

Figure 2 shows the calculated κ_{hBN} (solid red [lower] curve) as a function of temperature, T, compared with the measured data[10] (black diamonds). The only adjustable parameter in the model is L, for which a value of $L = 2$ μm ($L_{\rm eff} = 1.4$ μm) gives a reasonably good fit to the measured data.[33]

The peak and subsequent decrease in κ_{hBN} with increasing T indicates that three-phonon scattering becomes dominant. Similar behavior is obtained for an isotopically pure system,

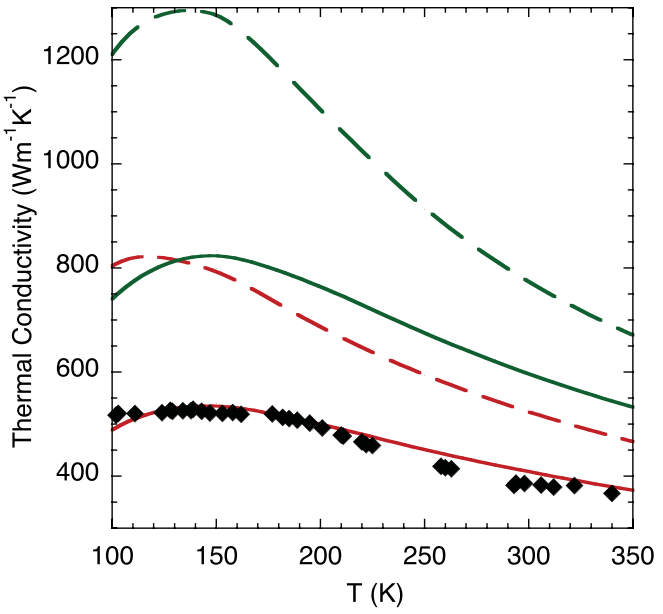

FIG. 2. (Color online) The solid red (lowest) curve shows the calculated κ_L of h-BN as a function of temperature, T, compared with measured values (black diamonds). The dashed red (lower) curve shows the κ_L for isotopically pure h-BN. The solid green (higher) curve gives the calculated κ_L for naturally occurring SLBN, whereas the dashed green (highest) curve shows calculated κ_L for isotopically pure SLBN.

where all boron atoms are ^{11}B (dashed red [lower] curve), with a ∼30% enhancement in κ_{hBN} at 300 K and almost a 70% increase around 100 K. Note that the 300 K value of ∼520 $Wm^{-1}K^{-1}$ is still much lower than κ_{graphite}, which contains 1.1% ^{13}C. We find that the difference stems primarily from the overall lower acoustic phonon frequencies in h-BN. Specifically, the Brillouin zone center curvature of the ZA branch is 29% smaller in SLBN than in graphene, whereas the TA and LA velocities are 27% and 13% smaller, respectively. The lower phonon frequencies enter Eq. (3) resulting in stronger phonon-phonon scattering rates Eq. (2) and lower κ_L.

The solid and dashed green (upper) curves show the calculated κ_L for SLBN (κ_{SLBN}) for the naturally occurring and the isotopically pure systems. The same value of $L = 2\ \mu$m has been used as for the bulk. In both cases, κ_{SLBN} is much higher than κ_{hBN}. This enhancement occurs primarily because of a selection rule in 2D crystals, such as SLBN and graphene, connected to the underlying reflection symmetry perpendicular to the layer,[5,7] which causes the matrix elements Eq. (4) to vanish for all three-phonon processes having an odd number of ZA phonons. The resulting strong restriction of the phase space available for phonon-phonon scattering increases ZA phonon lifetimes and enhances their already dominant contribution to κ_{SLBN}. This selection rule is broken by the interaction between the atoms in different layers, and the additional phonon-phonon scattering results in decreased κ_{hBN}.[13]

In layered materials such as h-BN and graphite, larger crystallite size increases κ_L.[10] To highlight this point and to illustrate the relative strengths of three-phonon scattering and that due to isotopes, Fig. 3 shows the calculated κ_{SLBN} at 300 K as a function of L, including: 1) only boundary and isotopic impurity scattering: κ_L^{iso} (dashed blue [highest] curve); 2) boundary and phonon-phonon scattering: κ_L^{pure} (solid red [upper] curve; this is the isotopically pure case); and 3) boundary, isotopic impurity, and phonon-phonon scattering: κ_L^{nat} (solid black [lower] curve). This corresponds to naturally occurring boron isotope concentrations. For comparison, the dashed gray (lowest) curve shows κ_{hBN}. It is evident that κ_L^{iso} is considerably larger than κ_L^{pure}, demonstrating that phonon-phonon scattering is much stronger than isotopic scattering around room temperature, even for the high isotope impurity concentration. We note the extremely high values of κ_L^{pure} (617–1107 $Wm^{-1}K^{-1}$ for $L = 1$–$10\ \mu$m) and the added enhancement obtained with increasing L: The $L = 1\ \mu$m ($L = 10\ \mu$m) value is 66% (144%) larger than κ_{hBN} for the same L.

Figure 4 shows the percent enhancement in κ_L, $P = (\kappa_L^{\text{pure}}/\kappa_L^{\text{nat}} - 1) \times 100\%$, due to isotopic enrichment as a function of T for different values of L. For fixed L, P rises as T decreases from 300 K because of the weakening phonon-phonon scattering. The isotope scattering then plays a more important role in limiting κ_L, so its removal causes greater enhancement. At low temperature, P drops because only low-frequency phonons are thermally populated, so the stronger frequency dependence of the isotopic scattering (see Eq. (5)) compared with the boundary scattering causes the latter to dominate as $T \to 0$.

Most striking in Fig. 4 are the successively larger peaks that form with increasing L. In this temperature range, the isotope scattering is strongest relative to the combined boundary and phonon-phonon scattering. The additional enhancement with increasing L reflects the weakening of the boundary scattering for the larger systems. At 300 K, this effect is modest, with P ranging from 26% for $L = 1\ \mu$m to 37% for $L = 10\ \mu$m. In contrast, the peak enhancements range from about 40% for $L = 1\ \mu$m to 200% for $L = 10\ \mu$m.

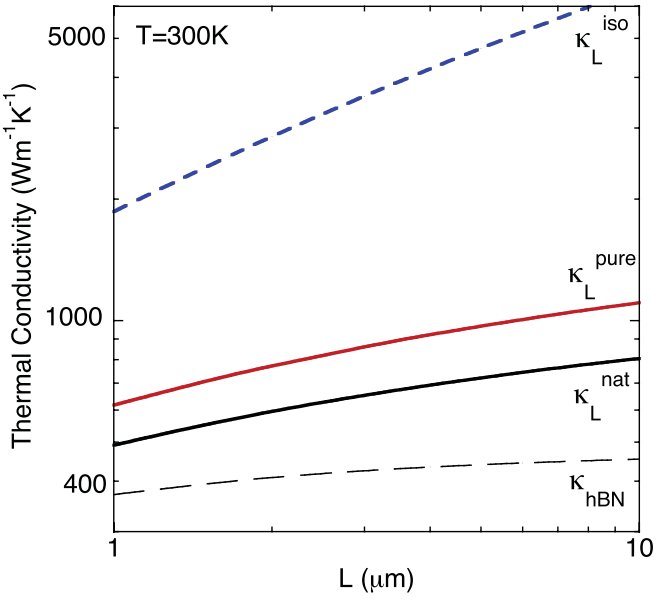

FIG. 3. (Color online) κ_L of SLBN at T = 300 K as a function of L, including boundary and isotope scattering (dashed blue [highest] curve), boundary and phonon-phonon scattering (solid red [upper] curve), and boundary, isotope, and phonon-phonon scattering (solid black [lower] curve). Also shown is κ_{hBN} (dashed gray curve).

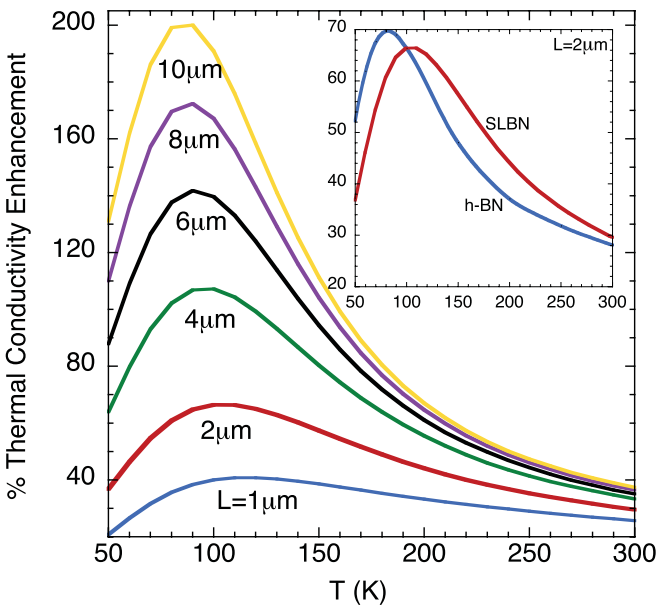

FIG. 4. (Color online) Percent enhancement, P, of κ_L in isotopically pure SLBN compared with naturally occurring SLBN as a function of T for different values of L. Inset compares P for SLBN and h-BN for $L = 2\ \mu$m.

Recently, the isotope effect has been observed in 10-μm-long multiwalled BNNTs in the range of about 100 K to 300 K.[12] The P extracted from this data exhibits a surprisingly weak dependence on T. Recent theoretical work[34] was able to match the κ_L data for both the naturally occurring and isotopically enriched samples, but only by assuming weak phonon-phonon scattering. This assumption would preclude a fit to the high T data for bulk h-BN shown in Fig. 2, yielding instead much larger than observed κ_{hBN}. Furthermore, strongly T-dependent isotope effects qualitatively similar to that shown in Fig. 4 have been observed in bulk materials.[35–37] It is notable that in bulk h-BN, which is a closer representation of multiwalled BNNTs, P shows a weaker T dependence over most of the measured range of Ref. 12, and its peak lies below this range (see Fig. 4 inset). Finally, the measured κ_Ls of multiwalled carbon nanotubes (MWCNTs) in Ref. 12 are almost the same as those for multiwalled BNNTs, which contrasts with the fivefold higher κ_L of graphite[11] compared with bulk h-BN.[10] Additional measurements on naturally occurring and isotopically enriched h-BN, SLBN, and BNNT systems, as well as on MWCNTs, are needed to further address this issue.

Two recent papers have investigated, theoretically, thermal transport in boron nitride nanoribbons (BNNR) using nonequilibrium Green's function[38] and molecular dynamics[39] approaches. Reference 38 finds BNNRs have similar κ_L to those of graphene nanoribbons. However, this work does not include phonon-phonon scattering. Reference 39 includes phonon-phonon scattering and finds much larger κ_L for graphene nanoribbons compared with h-BN nanoribbons, which is qualitatively consistent with our results. This highlights the important role played by phonon-phonon scattering in determining κ_L in both h-BN and graphene systems. Reference 39 has also developed a different Tersoff parameter set for h-BN layers, which shows similarly good agreement with the low-frequency portion of the measured in-plane phonon dispersion of bulk h-BN. We note that the effect on κ_L of isotope impurity scattering and its interplay with the anharmonic phonon-phonon scattering, which is a central part of the present work, is not considered in Refs. 38 or 39.

VI. SUMMARY AND CONCLUSIONS

Using an exact numerical solution of the phonon BTE, the κ_Ls of both naturally occurring and isotopically enriched SLBN and h-BN have been calculated. Good agreement is obtained with measured h-BN data, and the stronger phonon-phonon scattering identified in these systems explains why their κ_Ls are lower than those in graphene and graphite. The κ_L for SLBN is significantly larger than its bulk counterpart because of a reduction in phonon-phonon scattering in the 2D layer, resulting to a large extent from a symmetry-based selection rule. This feature gives SLBN one of the highest room temperature κ_Ls, other than those in the carbon allotropes. Additional enhancement is obtained from isotopic enrichment, which exhibits a strong peak as a function of temperature, with magnitude growing rapidly with crystallite size.

ACKNOWLEDGMENTS

D.A.B. acknowledges support from the National Science Foundation, under Grant No. 1066634. L.L. acknowledges support from the NRC/NRL Research Associateship Program and from DARPA. We also thank Natalio Mingo for useful discussions.

*Email address: broido@bc.edu

[1] C. R. Dean, A. F. Young, I. Meric, C. Lee, L. Wang, S. Sorgenfrei, K. Watanabe, T. Taniguchi, P. Kim, K. L. Shepard, and J. Hone, Nature Nanotech. **5**, 722 (2010).

[2] J. Xue, J. Sanchez-Yamagishi, D. Bulmash, P. Jacquod, A. Deshpande, K. Watanabe, T. Taniguchi, P. Jarillo-Herrero, and B. LeRoy, Nat. Mater. **10**, 282 (2011).

[3] A. A. Balandin, S. Ghosh, W. Bao, I. Calizo, D. Teweldebrhan, F. Miao, and C. N. Lau, Nano Lett. **8**, 902 (2008).

[4] S. Ghosh, I. Calizo, D. Teweldebrhan, E. P. Pokatilov, D. L. Nika, A. A. Balandin, W. Bao, F. Miao, and C. N. Lau, Appl. Phys. Lett. **92**, 151911 (2008).

[5] J. H. Seol, I. Jo, A. L. Moore, L. Lindsay, Z. H. Aitken, M. T. Pettes, X. Li, Z. Yao, R. Huang, D. A. Broido, N. Mingo, R. S. Ruoff, and L. Shi, Science **328**, 213 (2010).

[6] W. Cai, A. L. Moore, Y. Zhu, X. Li, S. Chen, L. Shi, and R. S. Ruoff, Nano Lett. **10**, 1645 (2010).

[7] L. Lindsay, D. A. Broido, and N. Mingo, Phys. Rev. B **82**, 115427 (2010).

[8] S. Chen, A. L. Moore, W. Cai, J. W. Suk, J. An, C. Mishra, C. Amos, C. W. Magnuson, J. Kang, L. Shi, and R. Ruoff, ACS Nano **5**, 321 (2011).

[9] A. A. Balandin, Nat. Mater. **10**, 569 (2011).

[10] E. K. Sichel, R. E. Miller, M. S. Abrahams, and C. J. Buiocchi, Phys. Rev. B **13**, 4607 (1976).

[11] Y. S. Touloukian, editor, *Thermal Conductivity, The TPRC data series* (IFI/Plenum, New York, 1970).

[12] C. W. Chang, A. M. Fennimore, A. Afanasiev, D. Okawa, T. Ikuno, H. Garcia, D. Li, A. Majumdar, and A. Zettl, Phys. Rev. Lett. **97**, 085901 (2006).

[13] L. Lindsay, D. A. Broido, and N. Mingo, Phys. Rev. B **83**, 235428 (2011).

[14] P. G. Klemens, J. Wide Bandgap Mater. **7**, 332 (2000).

[15] P. G. Klemens, Int. J. Thermophys. **22**, 265 (2001).

[16] W. Jang, Z. Chen, W. Bao, C. N. Lau, and C. Dames, Nano Lett. **10**, 3909 (2010).

[17] D. Pacilé, J. C. Meyer, Ç. Ö. Girit, and A. Zettl, Appl. Phys. Lett. **92**, 133107 (2008).

[18] W.-Q. Han, L. Wu, Y. Zhu, K. Watanabe, and T. Taniguchi, Appl. Phys. Lett. **93**, 223103 (2008).

[19] C. Jin, F. Lin, K. Suenaga, and S. Iijima, Phys. Rev. Lett. **102**, 195505 (2009).

[20] J. Tersoff, Phys. Rev. B **37**, 6991 (1988).

[21] J. Serrano, A. Bosak, R. Arenal, M. Krisch, K. Watanabe, T. Taniguchi, H. Kanda, A. Rubio, and L. Wirtz, Phys. Rev. Lett. **98**, 095503 (2007).

[22] W. Paszkowicz, J. B. Pelka, M. Knapp, T. Szyszko, and S. Podsiadlo, Appl. Phys. A **75**, 431 (2001).

[23] G. Kern, G. Kresse, and J. Hafner, Phys. Rev. B **59**, 8551 (1999).

[24]L. Lindsay and D. A. Broido, Phys. Rev. B **81**, 205441 (2010).
[25]K. H. Michel and B. Verberck, Phys. Rev. B **83**, 115328 (2011).
[26]N. Marom, J. Bernstein, J. Garel, A. Tkatchenko, E. Joselevich, L. Kronik, and O. Hod, Phys. Rev. Lett. **105**, 046801 (2010).
[27]D. J. Ecsedy and P. G. Klemens, Phys. Rev. B **15**, 5957 (1977).
[28]S. I. Tamura, Phys. Rev. B **27**, 858 (1983).
[29]I. Savić, N. Mingo, and D. A. Stewart, Phys. Rev. Lett. **101**, 165502 (2008).
[30]G. Stoltz, M. Lazzeri, and F. Mauri, J. Phys. Condens. Matter **21**, 245302 (2009).
[31]N. Mingo and D. A. Broido, Nano Lett. **5**, 1221 (2005).
[32]E. Munoz, J. Lu, and B. Yakobson, Nano Lett. **10**, 1652 (2010).
[33]This value is somewhat larger than the quoted crystallite size of about 1 mm in Ref. 10, reflecting that L is not a precise measure of this size.
[34]D. A. Stewart, I. Savić, and N. Mingo, Nano Lett. **9**, 81 (2009).
[35]L. Wei, P. K. Kuo, R. L. Thomas, T. R. Anthony, and W. F. Banholzer, Phys. Rev. Lett. **70**, 3764 (1993).
[36]A. V. Inyushkin, A. N. Taldenkov, A. M. Gibin, A. V. Gusev, and H.-J. Pohl, Phys. Status Solidi C **1**, 2995 (2004).
[37]M. Asen-Palmer, K. Bartkowski, E. Gmelin, M. Cardona, A. P. Zhernov, A. V. Inyushkin, A. Taldenkov, V. I. Ozhogin, K. M. Itoh, and E. E. Haller, Phys. Rev. B **56**, 9431 (1997).
[38]T. Ouyang, Y. Chen, Y. Xie, K. Yang, Z. Bao, and J. Zhong, Nanotechnology **21**, 245701 (2010).
[39]C. Sevik, A. Kinaci, J. B. Haskins, and T. Cagın, Phys. Rev. B **84**, 085409 (2011).